Journal of Materials Chemistry A

COMMUNICATION

View Article Online
View Journal | View Issue

Cite this: J. Mater. Chem. A, 2017, 5, 1400

Received 14th September 2016
Accepted 3rd December 2016

DOI: 10.1039/c6ta07990c

www.rsc.org/MaterialsA

Expanding metal cation options in polymeric anion exchange membranes†

Michael T. Kwasny and Gregory N. Tew*

Here we present the synthesis of new metal-containing ROMP-based anion exchange membranes (AEMs) incorporating either ruthenium, nickel, or cobalt. To accomplish this, homoleptic norbornene monomers were synthesized, cross-linked, and compared to systems previously synthesized, which featured heteroleptic ruthenium-containing monomers. This produced AEMs with varying metal cations, in an effort to elucidate the effect different metals have on AEM properties. The metal had minimal effect on water uptake and mechanical properties, while also maintaining excellent chemical stability. Conductivity, however, appeared to change as the metal changed, with the nickel-cation-containing AEM performing the best among all equivalent metal cations studied. These results indicate that metal-cation-based AEMs need not be limited to ruthenium.

Anion exchange membrane fuel cells (AEMFCs) have garnered interest over the past decade as a potential substitute for proton exchange membrane fuel cells (PEMFCs). Despite the success of PEMFCs in applications like generators and power plants, drawbacks such as high cost due to the required use of precious metal catalysts and perfluorinated polymers restrict their widespread implementation.[1–4] AEMFCs offer a potential alternative to PEMFCs, with reduction in overall cost, a wider range of potential fuels, and improved oxygen reduction kinetics.[1,5–7] Even so, anion exchange membranes (AEMs), the conducting membrane in an AEMFC, must overcome their own shortcomings before they can become commercially feasible. One such issue is the trade-off between conductivity and mechanical stability, which arises due to the water uptake in AEMs. While the water absorbed into the membrane helps facilitate anion conductivity by improving mobility, high water content also leads to weaker and mechanically unstable membranes.[1,8–11] Traditionally, the water uptake in membranes is lowered by reducing the relative amount of cations in the membrane; however, this also reduces the ion exchange capacity (IEC) of the material, thereby lowering the ion conductivity.[10,12]

Another problem facing AEMs is the alkaline promoted degradation of the commonly used cationic quaternary ammonium group.[6,11,13–15] In order to improve stability, numerous cation systems have been studied over the years, such as quaternary ammonium without β-hydrogens,[16–18] quaternary guanidinium,[19] imidazolium,[15] phosphonium,[20] and a metal–ligand complex.[9,21,22] Of these, metal cations are a distinct alternative to organic cations due to their robust stability as well as their higher valence and subsequent association of multiple anions.[23] One promising example from our own group was a ROMP-based AEM platform made through the gelation of norbornene functionalized ruthenium–terpyridine monomers, which resulted in mechanically robust and highly conductive membranes.[9,22] Ruthenium was initially chosen due to its well-known thermal and chemical stability; however, as seen in Fig. 1, ruthenium is a rare metal and thus may not be the best choice for large scale fuel cell production.[23–26] Therefore, expanding this approach to incorporate more readily available and stable metal–terpyridine complexes, featuring nickel or cobalt, would significantly improve the feasibility of these metal-cation-based AEMs.[25–27]

When designing metal cation containing AEMs there are a number of parameters to consider, including the redox potential of the metal. If the metals are active within the operation range of the AEMFC, then potentially detrimental side reactions can occur.[1,28] However, it has been shown that all three metal–terpyridine complexes (ruthenium, nickel, cobalt) contain redox potentials outside of the range for AEMs and thus should not be active (Table S1†).[29–34] In addition, due to the fast equilibrium kinetics of nickel– and cobalt–terpyridine bonds, heteroleptic complexes with these metals are difficult to isolate.[27,35,36] Thus, AEMs derived from homoleptic ruthenium, nickel, and cobalt complexes, as well as a heteroleptic ruthenium complex which primarily serves as a control and reference to previous work,[22] were synthesized and compared to determine the effect different metal-cations have on AEM properties.

Department of Polymer Science and Engineering, University of Massachusetts Amherst, Amherst, MA 01003, USA. E-mail: tew@mail.pse.umass.edu

† Electronic supplementary information (ESI) available. See DOI: 10.1039/c6ta07990c

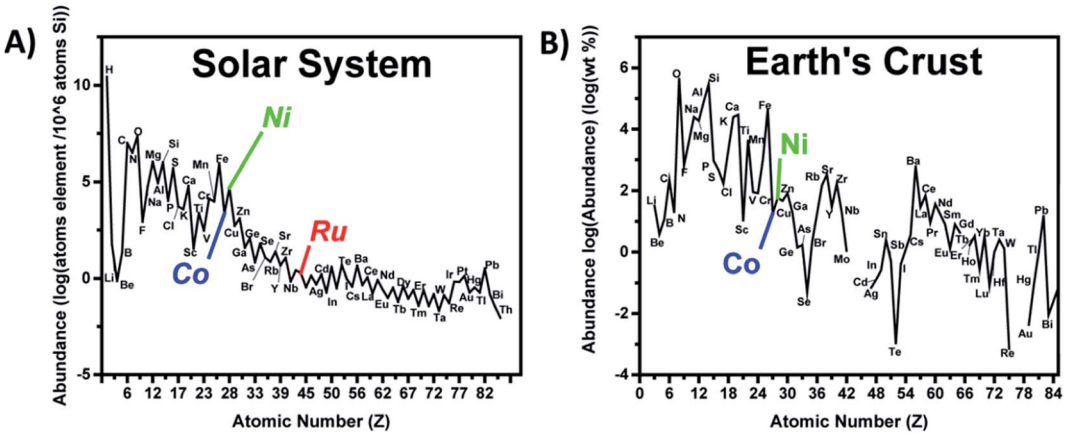

Fig. 1 Plot showing the natural abundance of all elements (A) in the solar system,[25] and (B) in Earth's crust.[26] Ruthenium abundance in the Earth's crust was minimal and thus not provided.

The synthesis of all monomers (**M1–M4**) is shown in Scheme 1. **M1** is a heteroleptic, mono(norbornene) functionalized, ruthenium–terpyridine complex, whereas **M2–M4** are homoleptic, bis(norbornene) functionalized terpyridine complexes containing either ruthenium, nickel, or cobalt for **M2**, **M3**, and **M4**, respectively. All monomer and subsequent AEM syntheses followed adaptions from our previously reported procedures.[9,22] It was observed that the mono(norbornene) functionalized **M1** was water soluble, but the bis(norbornene) functionalized **M2–M4** became completely water insoluble. The subsequent AEMs **1–4**, derived from their corresponding monomers, were synthesized using Grubbs' second generation catalyst, G2, in a methanol/chloroform solvent mixture (Scheme 2). AEM **1** was formed with the crosslinker dicyclopentadiene (DCPD), while AEMs **2–4** were formed with both DCPD and norbornene. This was done to ensure that both the molar ratio of charged to uncharged monomers as well as non-crosslinkers to crosslinkers remained 1 : 5.

The resulting membranes were first studied for their water uptake, as measured by comparing the masses of the hydrated

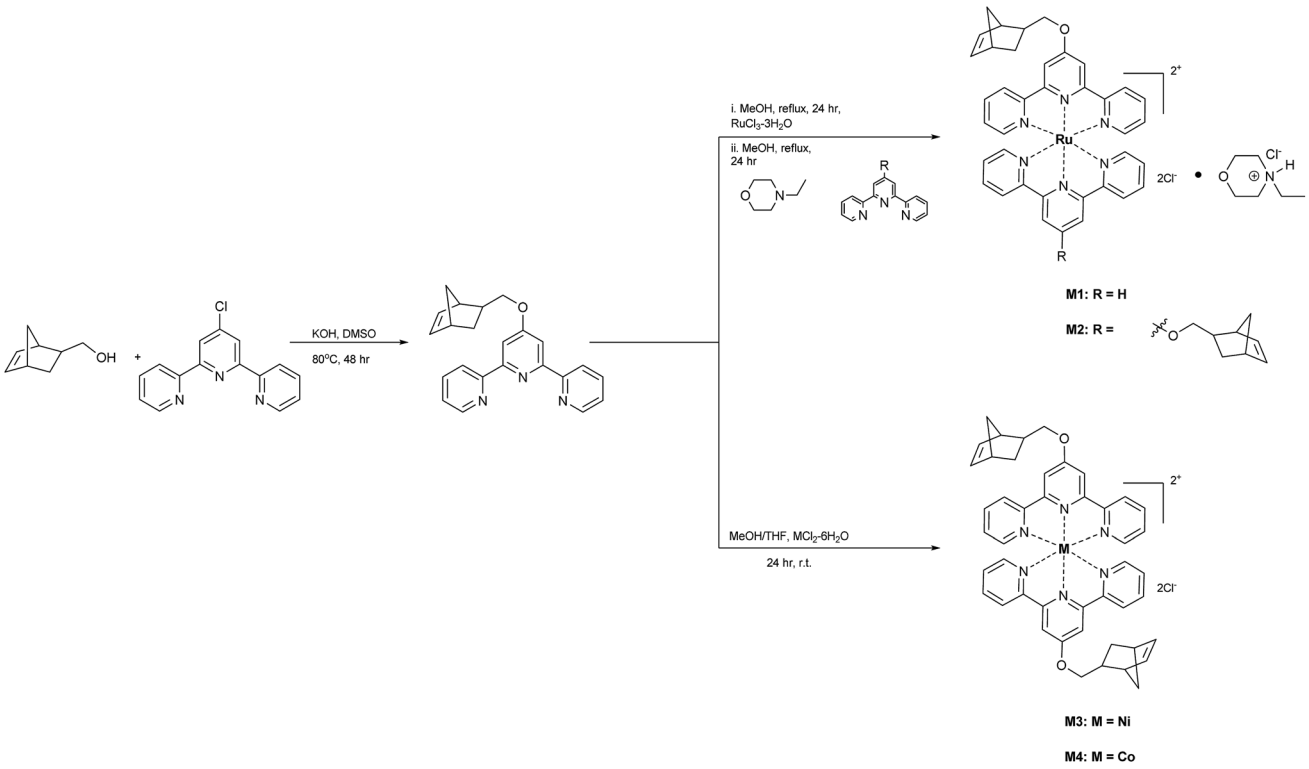

Scheme 1 Synthesis of monomers M1–M4, where M1 contains the heteroleptic ruthenium complex and M2, M3 and M4 all contain a homoleptic complex, but with different metals.

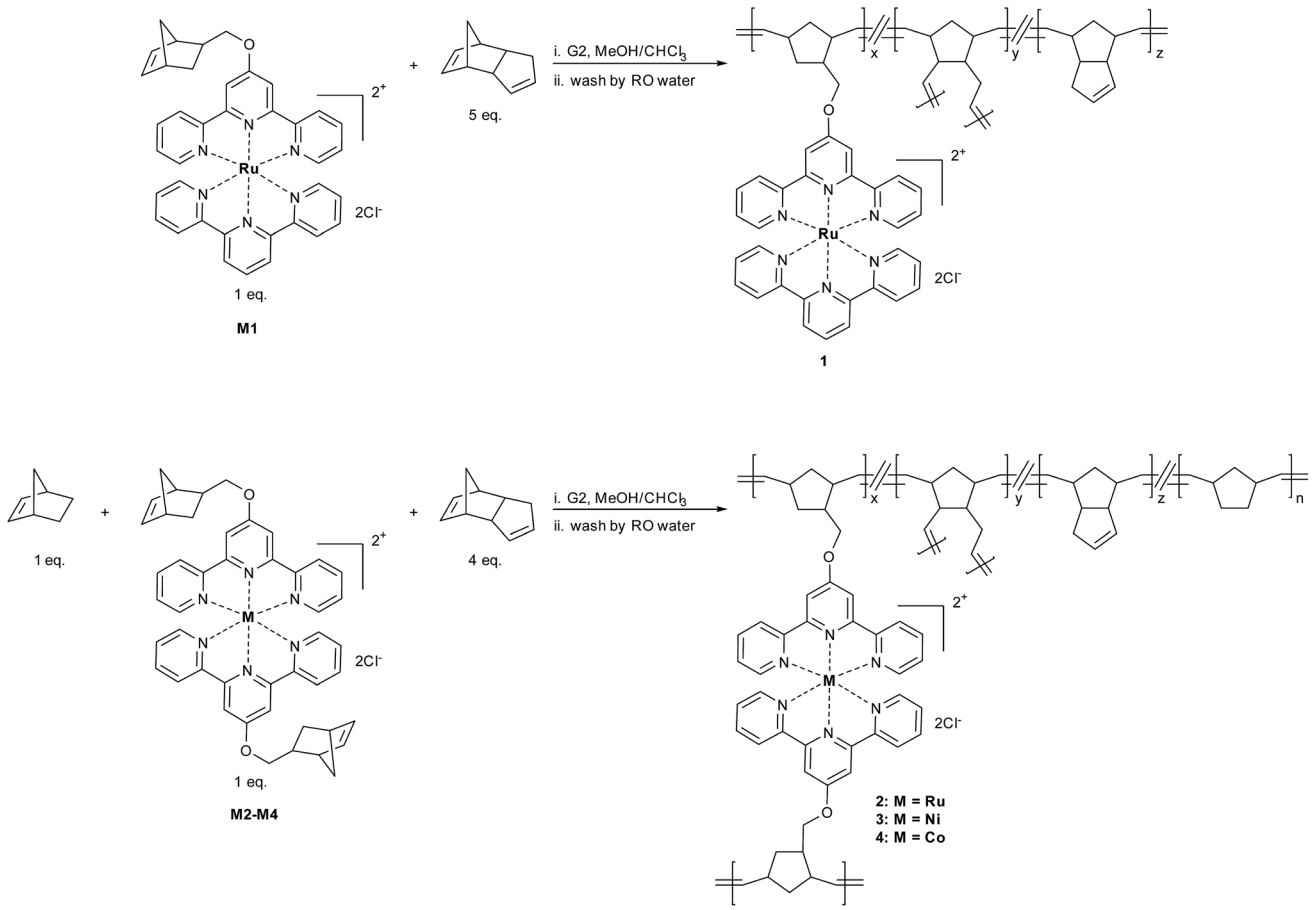

Scheme 2 Synthesis of AEMs **1–4** from monomers **M1–M4**, respectively, with AEMs **2–4** containing norbornene to keep molar equivalents of the cations consistent between all membranes. The addition of norbornene for AEMs **2–4** also keeps the ratio of crosslinker to non-crosslinker the same. Molar equivalent for each monomer is indicated below the chemical structure.

and dried membranes. Fig. 2 shows that AEM **1** had the highest water uptake, 230%, *versus* 30–35% for **2–4**, with exact values shown in Table 1. The swelling data indicates that changing the transition metal appears to have little effect on the amount of water absorbed into the network, but that the chemistry surrounding the cationic unit plays a crucial role. This is supported by the UV-vis spectra of each monomer in DI water (Fig. S1†), showing that **M1** had very strong absorbance in the UV region, but **M2–M4** showed very low absorbance. The low absorbance for **M2–M4** is due to the fact that these monomers never dissolved in the water, showing their hydrophobicity. By making the monomers more hydrophobic with the addition of the extra norbornene, AEMs with higher potential IECs but reduced water uptake were produced.

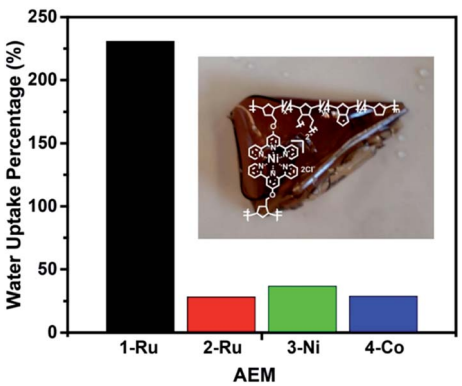

Fig. 2 Water uptake values for all AEMs, measured by weighing the swollen gel and the corresponding dried membrane. Inset image is of swollen AEM **3**.

The lack of alkaline stability is a major limitation for all AEM materials. Therefore, all four AEMs were tested for their alkaline stability by monitoring their mass loss, as measured in the dried state, after incubation in an aqueous 2 M KOH solution at 80 °C for up to 48 hours (Fig. 3). As Fig. 3 indicates, AEM **1** had 75% mass remaining after the first six hours, which then stabilized at 72% after 48 hours. Since previous reports have demonstrated the alkaline stability of ruthenium complexes, this mass loss observed here was most likely related to a loss of sol fraction.[22] To test this theory, AEM **1** was tested in both less harsh conditions (1 M NaOH at 80 °C) as well as in multiple incubations in 2 M KOH. It showed similar mass loss even in this slightly milder condition (Fig. S2†), but showed no further mass loss in subsequent incubations in KOH (Fig. S3 and S4†). In addition, **1** showed a lower gel fraction than **2–4** (Table S2†),

Table 1 Membrane properties for all AEMs

AEM	Theoretical IEC[a] (mmol g^{-1})	Experimental IEC (mmol g^{-1})	Water uptake[b] (%)	Mass remaining[c] (%)	$\sigma^*(Cl^-)_{80°C}$[d] (mS cm^{-1})	Tensile stress at break[e] (MPa)	Tensile strain at break[e] (%)
1	1.24	1.08 ± 0.11	231	72	3.40	27 ± 15	8.1 ± 2.5
2	1.19	0.89 ± 0.51	28.0	94	0.92	37 ± 22	13 ± 5.8
3	1.35	0.49 ± 0.11	36.0	98	2.40	45 ± 12	7.9 ± 2.9
4	1.35	0.56 ± 0.29	29.0	99	0.30	56 ± 17	8.3 ± 3.5

[a] Theoretical IEC calculated based on the chemical structure. [b] Liquid water uptake in the Cl^- form at room temperature, where water uptake = $[(m_{wet} - m_{dry})/m_{dry}]$. [c] Percent of dried mass remaining with membranes in the OH^- form after 48 h at 80 °C. [d] Normalized Cl^- conductivity at 95% relative humidity and 80 °C ($\sigma^*_{80°C} = \sigma_{80°C}/IEC_{theo}$). [e] Obtained using dynamic mechanical analysis in the Cl^- form and in the dried state. Average values, with errors, from three trials are shown.

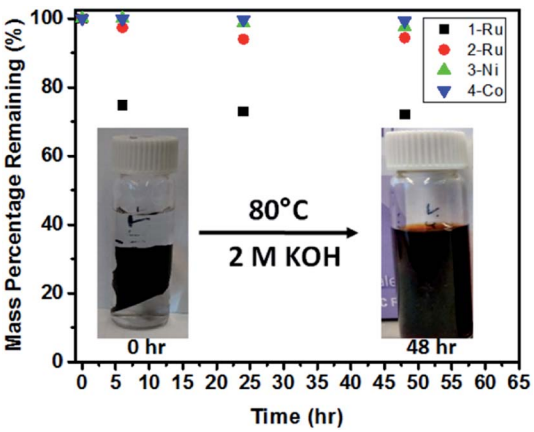

Fig. 3 Mass stability in aqueous 2 M KOH solution at 80 °C. The data indicates amount of mass remaining after a given time. Inset image shows how the aqueous KOH solution removes ruthenium from AEM **1** over the 48 hours.

which supports the idea that the observed mass lost for AEM **1** is almost certainly due to sol fraction not removed during the initial work-up as opposed to actual degradation of the membrane, especially since degradation would continue in subsequent incubations.

Further, AEMs **2–4** showed excellent stability after the full 48 hours of incubation. AEM **2**, containing ruthenium, showed 94% of its mass remaining after incubation; AEMs **3** and **4**, containing nickel and cobalt, respectively, showed greater than 98% mass remaining. This shows that despite introducing more labile metal–ligand bonds into these membranes with nickel and cobalt, robust chemical stability was maintained.

To test mechanical stability, samples were cut into rectangular films, dried, and tested using dynamic mechanical analysis (DMA) at a preload force of 0.001 N and a force ramp of 1 N min^{-1} to obtain the stress and strain at break. An example curve can be seen in Fig. 4, with average stresses and strains at break reported in Table 1. All samples showed similar stresses and strains with a stress at break ranging from 27–56 MPa and a strain at break ranging from 8–13%. Thus all samples, regardless of monomer chemistry or metal incorporated, have comparable mechanical properties both within this series as well as with respect to literature values.[11,14]

To determine how conductivity varied with metal ion, chloride conductivity was measured as a function of temperature at 95% relative humidity (Fig. 5). As expected, all samples showed an increase in conductivity with temperature, but differed between samples, with AEMs **1** and **3** performing the best. In order to adjust for the IEC of each membrane, a relative conductivity at 80 °C, $\sigma^*_{80°C}$, was calculated by dividing the observed conductivity by the theoretical IEC, with values reported in Table 1. The theoretical IEC was used for this calculation to provide a theoretical conductivity comparison in ideal AEMs, however if the experimental IEC values were used the relative conductivity would just be larger.

AEM **1** showed the highest relative conductivity, with a $\sigma^*_{80°C}$ of 3.4 mS cm^{-1}. This is unsurprising, since **1** also demonstrated the highest water uptake. It is, however, noteworthy that the relative conductivity changed between AEMs **2–4**. The nickel-containing AEM **3** showed the highest conductivity of 2.4 mS cm^{-1}, while **2** (Ru) showed a moderate conductivity of 0.92 mS cm^{-1} and **4** (Co) showed the lowest conductivity of 0.3 mS cm^{-1}. Furthermore, the experimental IEC, determined through back titration and shown in Table 1, strengthens the argument that nickel appears to perform the best since it had a lower metal content as compared to AEMs **1**, **2**, and **4**, yet higher

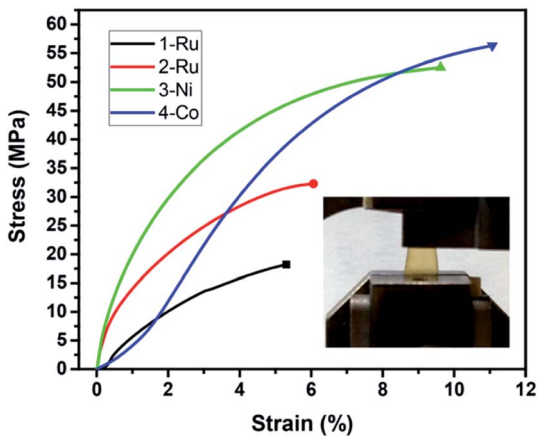

Fig. 4 Example mechanical data for all AEMs using dynamic mechanical analysis. Symbol at the end of the curve indicates stress and strain at break for each sample. Inset image shows AEM **3** in the DMA apparatus.

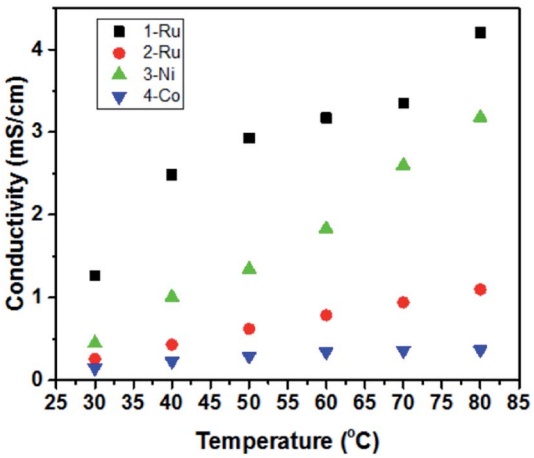

Fig. 5 Cl^- conductivity for all AEMs as a function of temperature in 95% relative humidity. All samples show an increase in conductivity as temperature increases.

conductivity. These results highlight the potential of nickel containing AEMs with AEM **3** rivaling, or surpassing, the conductivity of AEM **1** at a considerably reduced water content, which is advantageous. Moreover, nickel is orders of magnitude more abundant than ruthenium, greatly improving the accessibility of metal-based AEMs.

New metal-containing monomers, utilizing ruthenium, nickel, and cobalt, were synthesized and incorporated into novel AEMs. Hydrophobic, homoleptic metal-based AEMs were synthesized, which demonstrated minimal water uptake as compared to the heteroleptic ruthenium-based AEM. Despite the low water uptake, the nickel-containing AEM **3** was comparable to AEM **1** in terms of conductivity and outperformed the analogous ruthenium- and cobalt-containing AEMs, demonstrating the importance different metal cations have on AEM performance. Considering the high mechanical and chemical stability, low water content, and comparable conductivity, nickel provides a promising alternative to ruthenium for metal-cation-based AEMs, making them more feasible for future fuel cell applications.

Conflict of interest

The authors declare no competing financial interests.

Acknowledgements

This work was funded by the NSF NRT program DGE-1545399, NSF GAANN Fellowship DoED P200A150276 and through MRSEC grant DMR-0820506. Mass Spectral data were obtained at the University of Massachusetts Mass Spectrometry Center. The authors thank Mr Joel Sarapas and Mr Nicholas Posey for their assistance in preparing the manuscript. The authors also thank Prof. Mark Touminen and Mr Ramesh Adhikari, for maintaining and allowing access to private instrumentation. Special thanks goes to Mr Matthew Lampe for his assistance in dynamic mechanical analysis.

References

1 M. A. Hickner, A. M. Herring and E. B. Coughlin, *J. Polym. Sci., Part B: Polym. Phys.*, 2013, **51**, 1727–1735.
2 H.-W. Zhang, D.-Z. Chen, Y. Xianze and S.-B. Yin, *Fuel Cells*, 2015, **15**, 761–780.
3 L. Zhu, T. J. Zimudzi, N. Li, J. Pan, B. Lin and M. A. Hickner, *Polym. Chem.*, 2016, **7**, 2464–2475.
4 T. J. Peckham and S. Holdcroft, *Adv. Mater.*, 2010, **22**, 4667–4690.
5 J. Ran, L. Wu, B. Wei, Y. Chen and T. Xu, *Sci. Rep.*, 2014, **4**, 6486.
6 G. Couture, A. Alaaeddine, F. Boschet and B. Ameduri, *Prog. Polym. Sci.*, 2011, **36**, 1521–1557.
7 G. He, Z. Li, J. Zhao, S. Wang, H. Wu, M. D. Guiver and Z. Jiang, *Adv. Mater.*, 2015, **27**, 5280–5295.
8 M. L. Disabb-Miller, Z. D. Johnson and M. A. Hickner, *Macromolecules*, 2013, **46**, 949–956.
9 M. L. Disabb-Miller, Y. Zha, A. J. DeCarlo, M. Pawar, G. N. Tew and M. a. Hickner, *Macromolecules*, 2013, **46**, 9279–9287.
10 X. Ren, S. C. Price, A. C. Jackson, N. Pomerantz and F. L. Beyer, *ACS Appl. Mater. Interfaces*, 2014, **6**, 13330–13333.
11 J. Pan, L. Zhu, J. Han and M. A. Hickner, *Chem. Mater.*, 2015, **27**, 6689–6698.
12 S. P. Ertem, T.-H. Tsai, M. M. Donahue, W. Zhang, H. Sarode, Y. Liu, S. Seifert, A. M. Herring and E. B. Coughlin, *Macromolecules*, 2016, **49**, 153–161.
13 J. B. Edson, C. S. Macomber, B. S. Pivovar and J. M. Boncella, *J. Membr. Sci.*, 2012, **399–400**, 49–59.
14 J. Ran, L. Wu, Q. Ge, Y. Chen and T. Xu, *J. Membr. Sci.*, 2014, **470**, 229–236.
15 B. Wang, W. Sun, F. Bu, X. Li, H. Na and C. Zhao, *Int. J. Hydrogen Energy*, 2016, **41**, 3102–3112.
16 N. J. Robertson, H. A. Kostalik, T. J. Clark, P. F. Mutolo, H. D. Abruña and G. W. Coates, *J. Am. Chem. Soc.*, 2010, **132**, 3400–3404.
17 H. A. Kostalik, T. J. Clark, N. J. Robertson, P. F. Mutolo, J. M. Longo, H. D. Abruña and G. W. Coates, *Macromolecules*, 2010, **43**, 7147–7150.
18 T. J. Clark, N. J. Robertson, H. A. Kostalik IV, E. B. Lobkovsky, P. F. Mutolo, H. D. Abruña and G. W. Coates, *J. Am. Chem. Soc.*, 2009, **131**, 12888–12889.
19 J. Wang, S. Li and S. Zhang, *Macromolecules*, 2010, **43**, 3890–3896.
20 K. J. T. Noonan, K. M. Hugar, H. A. Kostalik, E. B. Lobkovsky, H. D. Abruña and G. W. Coates, *J. Am. Chem. Soc.*, 2012, **134**, 18161–18164.
21 S. Gu, J. Wang, R. B. Kaspar, Q. Fang, B. Zhang, E. Bryan Coughlin and Y. Yan, *Sci. Rep.*, 2015, **5**, 11668.
22 Y. Zha, M. L. Disabb-Miller, Z. D. Johnson, M. A. Hickner and G. N. Tew, *J. Am. Chem. Soc.*, 2012, **134**, 4493–4496.
23 K. A. Aamer and G. N. Tew, *Macromolecules*, 2007, **40**, 2737–2744.
24 J.-F. Gohy, B. G. G. Lohmeijer, S. K. Varshney and U. S. Schubert, *Macromolecules*, 2002, **35**, 7427–7435.

25 E. Anders and N. Grevesse, *Geochim. Cosmochim. Acta*, 1989, **53**, 197–214.
26 A. A. Yaroshevsky, *Geochem. Int.*, 2006, **44**, 48–55.
27 R. Hogg and R. G. Wilkins, *J. Chem. Soc.*, 1962, 341–350.
28 J. R. Varcoe and R. C. T. Slade, *Fuel Cells*, 2005, **5**, 187–200.
29 J. T. Ciszewski, D. Y. Mikhaylov, K. V. Holin, M. K. Kadirov, Y. H. Budnikova, O. Sinyashin and D. A. Vicic, *Inorg. Chem.*, 2011, **50**, 8630–8635.
30 K. Hutchison, J. C. Morris, T. A. Nile, J. L. Walsh, D. W. Thompson, J. D. Petersen and J. R. Schoonover, *Inorg. Chem.*, 1999, **38**, 2516–2523.
31 M. Maestri, N. Armaroli, V. Balzani, E. C. Constable and A. M. W. C. Thompson, *Inorg. Chem.*, 1995, **34**, 2759–2767.
32 J. P. Collin, S. Guillerez, J. P. Sauvage, F. Barigelletti, L. De Cola, L. Flamigni and V. Balzani, *Inorg. Chem.*, 1991, **30**, 4230–4238.
33 A. R. Guadalupe, D. A. Usifer, K. T. Potts, H. C. Hurrell, A. E. Mogstad and H. D. Abruna, *J. Am. Chem. Soc.*, 1988, **110**, 3462–3466.
34 J. M. Kelly, C. Long, C. M. O'Connell, J. G. Vos and A. H. A. Tinnemans, *Inorg. Chem.*, 1983, **22**, 2818–2824.
35 K. T. Potts, D. A. Usifer, A. Guadalupe and H. D. Abruna, *J. Am. Chem. Soc.*, 1987, **109**, 3961–3967.
36 K. T. Potts and D. A. Usifer, *Macromolecules*, 1988, **21**, 1985–1991.